Magnetic Tunnel Junctions Based on Ferroelectric Hf0.5Zr0.5O2 Tunnel Barriers

Wei, Yingfen; Matzen, Sylvia; Maroutian, Thomas; Agnus, Guillaume; Salverda, Mart; Nukala, Pavan; Chen, Qihong; Ye, Jianting; Lecoeur, Philippe; Noheda, Beatriz

IMPORTANT NOTE: You are advised to consult the publisher's version (publisher's PDF) if you wish to cite from it. Please check the document version below.

Document Version
Publisher's PDF, also known as Version of record

[Link to publication in University of Groningen/UMCG research database](#)

Letter   Editors' Suggestion

Magnetic Tunnel Junctions Based on Ferroelectric Hf$_{0.5}$Zr$_{0.5}$O$_2$ Tunnel Barriers

Yingfen Wei,[1] Sylvia Matzen,[2,*] Thomas Maroutian,[2] Guillaume Agnus,[2] Mart Salverda,[1]
Pavan Nukala,[1] Qihong Chen,[1] Jianting Ye,[1] Philippe Lecoeur,[2] and Beatriz Noheda[1,3,†]

[1]*Zernike Institute for Advanced Materials, University of Groningen, 9747 AG Groningen, Netherlands*
[2]*Centre for Nanoscience and Nanotechnology, CNRS UMR 9001, Université Paris-Sud, Université Paris-Saclay,
91120 Palaiseau, France*
[3]*CogniGron Center, University of Groningen, 9747 AG Groningen, Netherlands*

Ferroelectric tunnel barriers in between two ferromagnetic electrodes (multiferroic tunnel junctions, or MFTJs) hold great promise for future microelectronic devices. Here, we utilize Hf$_{0.5}$Zr$_{0.5}$O$_2$ (HZO) tunnel barriers with an ultralow thickness of only 2 nm, epitaxially grown on La$_{0.7}$Sr$_{0.3}$MnO$_3$ ferromagnetic bottom electrodes and with cobalt top electrodes. Both tunneling electroresistance and tunneling magnetoresistance effects are observed, demonstrating four nonvolatile resistance states in HZO-based junctions. The large band gap and excellent homogeneity of the HZO tunnel barriers enable a high yield of working devices, as well as devices with sizes of tens of micrometers. This allows working with fixed electrodes, as opposed to the use of scanning probes, bringing MFTJs closer to applications.

The concept of ferroelectric memory is by now mature [1]. The achievement of switchable ferroelectric polarization in ultrathin films has opened up possibilities for ferroelectric tunnel junctions (FTJs) [2–5]. Polarization switching of the ferroelectric barrier in a FTJ results in a change of the tunneling conductance, which is known as the tunnel electroresistance (TER) effect. This phenomenon has been observed in several systems, such as BaTiO$_3$ [6–8], Pb(Zr$_{0.2}$Ti$_{0.8}$)O$_3$ [9], PbTiO$_3$ [10], and BiFeO$_3$ [11,12]. Its origin has been mainly ascribed to three possible mechanisms [5]: (a) incomplete charge screening at ferroelectric-electrode interfaces affecting the potential barrier profile; (b) the change in the positions of ions at the interfaces after polarization reversal; and/or (c) the strain differences induced by the electric field in the ferroelectric barrier.

Nevertheless, the achievement of sufficiently thin ferroelectric films remains very challenging due to several issues, such as the difficulty of fully screening the surface polarization charges [13], the tendency of the films to form domain walls or other topological defects that cancel the net spontaneous polarization, the increase of the electric fields needed for polarization switching, or the increase in the leakage currents. In the past few years, intensive research has been conducted on hafnia- (hafnium-dioxide-) based thin films due to their unexpected ferroelectricity [14,15] and their complementary metal-oxide

semiconductor (CMOS) compatibility [16]. Unlike all other known ferroelectrics, in hafnia-based thin films, the ferroelectricity becomes more robust as the size is decreased and it disappears above a certain thickness, in the range of 10–30 nm [17]. Thus, hafnia-based thin films are highly promising as tunnel barriers for ferroelectric tunnel junctions. Moreover, amorphous hafnia is a high-k material that has been widely used as a gate insulator in the microelectronics industry [18], so these thin films have great potential for applications in the next generation of memories and logic devices, showing great advantages compared to conventional perovskite ferroelectrics.

Multiferroic tunnel junctions (MFTJs), with a ferroelectric tunnel barrier integrated between two magnetic electrodes, instead of a linear-dielectric barrier (as in magnetic tunnel junctions, MTJs), were proposed a decade ago [19] and have become a promising approach to the development of low-power, high-density, multifunctional, and nonvolatile memory devices [20,21]. A MFTJ exhibits four nonvolatile resistance states that can be achieved by external electric and magnetic field switching and are generated by the combination of the TER and tunneling magnetoresistance (TMR) effects. The TER originates from the partial screening of polarization charges, leading to a switchable electrostatic field across the ferroelectric, whereas the TMR originates in the dependence of the tunneling current on the parallel or antiparallel magnetization states between the two ferromagnetic electrode layers [22]. Previous studies on MFTJs have used ferroelectric tunnel barriers of BaTiO$_3$ or PbTiO$_3$/Pb(Zr, Ti)O$_3$ (PZT),

_____

*sylvia.matzen@u-psud.fr
†b.noheda@rug.nl

sandwiched between $La_{0.7}Sr_{0.3}MnO_3$ (LSMO) and Co magnetic electrodes [23–25].

Recently, several works on FTJs with hafnia barriers have been reported [26–31]. However, the hafnia-based barriers reported in MTJs are amorphous, undoped, and nonpolar [32,33]. In our recent work, crystalline rhombohedral $Hf_{0.5}Zr_{0.5}O_2$ (HZO) films have been grown epitaxially on (001)-LSMO (bottom electrode)/$SrTiO_3$ substrates and have shown ferroelectric switching with increasingly large remanent polarization values as the thickness decreases from 9 nm ($P_r = 18$ $\mu C/cm^2$) down to 5 nm ($P_r = 34$ $\mu C/cm^2$) [34]. Here, we report the integration of ferroelectric HZO tunnel barriers in MFTJs, showing four nonvolatile resistance states, as a combination of both TER and TMR effects.

Thin layers of ferroelectric HZO with a thickness of 2 nm are grown on LSMO-buffered STO substrates by pulsed-laser deposition [34]. On top of HZO films, 50-nm top Co ferromagnetic (FM) electrodes with a protective layer of Au (50 nm) are deposited by sputtering. MFTJs are created from the LSMO (FM)/HZO (FE)/Co (FM) stack. Junctions of different sizes (10×10 μm^2, 20×20 μm^2, and 30×30 μm^2) are fabricated by photolithography, chemically assisted ion-beam etching (IBE) controlled by a secondary-ion mass spectrometer (SIMS), and sputtering of metallic-top electrodes and a Si_3N_4 insulating layer in different steps. The cross-section scanning transmission electron microscopy (HAADF-STEM) image presented in Fig. 1(a) shows sharp interfaces between LSMO/rhombohedral (111)-oriented HZO layers [34] and polycrystalline Co [for an energy-dispersive x-ray spectroscopy (EDS) image, see Fig. S1 in the Supplemental Material [35]]. From the TEM images across different regions and atomic force microscopy (AFM) topography shown in Fig. S2 (see the Supplemental Material [35]), the roughness of the HZO film is estimated to be approximately 0.2 nm. A schematic view of a complete MFTJ device is shown in Fig. 1(b). The junctions are connected by wire bonding to chip carrier. The low temperature and magnetic field are applied using the Physical Properties Measurement System (PPMS) from Quantum Design. The electrical measurements are performed using a Keithley 237 source measurement unit and the electrical pulses are done with a Keithley 4200A-SCS parameter analyzer.
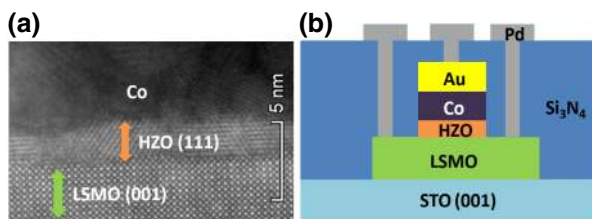

FIG. 1. (a) A HAADF-STEM cross-section image of a LMSO/HZO/Co stack. (b) A schematic drawing of the tunnel-junction devices used in this work.
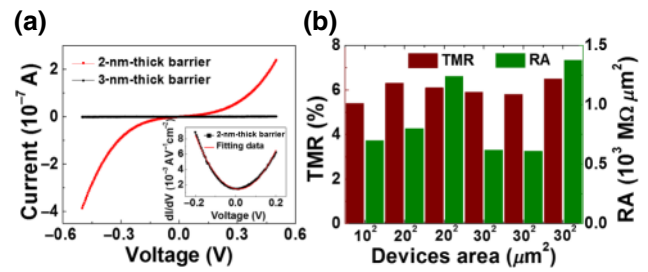

FIG. 2. (a) *I-V* curves at 300 K of 20×20 μm^2 junctions with 2-nm- and 3-nm-thick barriers. The inset shows the derivative of the *I-V* curve for the 2-nm barrier, with the parabolic Brinkman fit. (b) The TMR at 50 K and the resistance-area product (RA) for different device sizes (10×10 μm^2, 20×20 μm^2, and 30×30 μm^2) on the same sample with a 2-nm-thick HZO barrier.

The current-voltage (*I-V*) characteristics of 2-nm- and 3-nm-thick films with the same junction area (20×20 μm^2) are shown in Fig. 2(a). The current through the 3-nm-thick HZO film is too low (below 1 nA) to be reliably measured with our experimental setup and a thinner film is required for a tunneling junction. Indeed, the parabolic dependence of the differential conductance of the 2-nm film fitted by the Brinkman model [36] leads to a barrier height of 1.2 ± 0.1 eV with an asymmetry of 0.2 ± 0.1 eV (thus giving a height of approximately 1.3 eV on the Co side and approximately 1.1 eV on the LSMO side) and a barrier thicknesses of 1.5 ± 0.1 nm, indicating that the transport mechanism is direct tunneling through the HZO barrier. Due to the large band gap (5–6 eV) of HZO, the junction is very resistive even for ultrathin films, thus preventing leakage problems and improving the stability of the devices. All further measurements are performed on different devices with the same ultrathin 2-nm-thick barrier.

Junctions with different sizes are fabricated and six of them with a STO/LSMO/HZO (2-nm)/Co stack are connected to a chip carrier and measured. They all show TMR ratios between 5% and 7% under -0.2 V bias at a temperature of 50 K [Fig. 2(b)]. In addition, the resistance-area product (RA) is also quite constant for various device sizes, as shown in Fig. 2(b). This high reproducibility in the properties of the junctions proves the excellent quality of the HZO tunnel barrier, despite the domainlike nanostructure of the films [34].

The magnetic hysteresis loop *M-H* of a similar (but unpatterned) sample at 50 K is shown in Fig. 3(a), with the magnetic field applied along the in-plane [110] easy-axis direction of the LSMO. The magnetic switching of both LSMO and Co layers is clearly observed, showing coercive fields of around ± 50 Oe for LSMO and ± 250 Oe for Co. This difference allows for an antiparallel magnetic alignment between the two magnetic electrodes for intermediate magnetic fields. The resistance of such devices is measured as a function of the magnetic field under a bias of -0.2 V (applied to the top Co electrode)
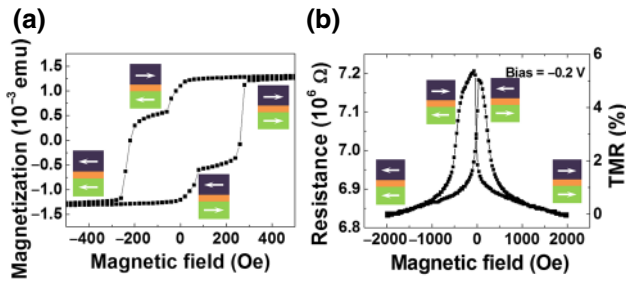
FIG. 3. (a) The *M-H* loop of an unpatterned sample measured at 50 K by superconducting-quantum-interference-device (SQUID) magnetometry along the in-plane [110] direction of the LSMO. (b) The TMR loop measured in a junction of size 10×10 μm^2 under a bias of -0.2 V at 50 K, with high (low) resistance in the antiparallel (parallel) state.

at a temperature of 50 K in a 10×10 μm^2 junction, for magnetic field cycling from 2000 Oe to -2000 Oe and back, along the [110] axis [Fig. 3(b)]. A higher-resistance state is measured in the antiparallel magnetic configuration when sweeping the field, displaying a positive TMR value of 5.4%, where the TMR is defined as $(R_{AP} - R_P)/R_P$, with R_{AP} and R_P the resistance values in the antiparallel and parallel states, respectively. This value is lower than the TMR reported for MTJs with perovskite barriers, such as SrTiO$_3$ [37,38], LaAlO$_3$ [39], or PbTiO$_3$ [40], probably due to the higher structural and chemical mismatch at the interface between the LSMO spin-polarized electrode and the HZO barrier.

The TMR effect decreases with increasing temperature and disappears above 250 K (Fig. 4), in agreement with most studies performed on other MFTJs with LSMO and Co electrodes [25], which could be a result of either the decrease of the spin polarization of LSMO at the interface with HZO and/or the spin-independent tunneling through impurity levels in the barrier activated upon increasing the temperature [41–45].

In the present case of a HZO barrier, we observe a resistance switching behavior as shown in Fig. 5(a). The resistance hysteresis loop indicates a memristive behavior,
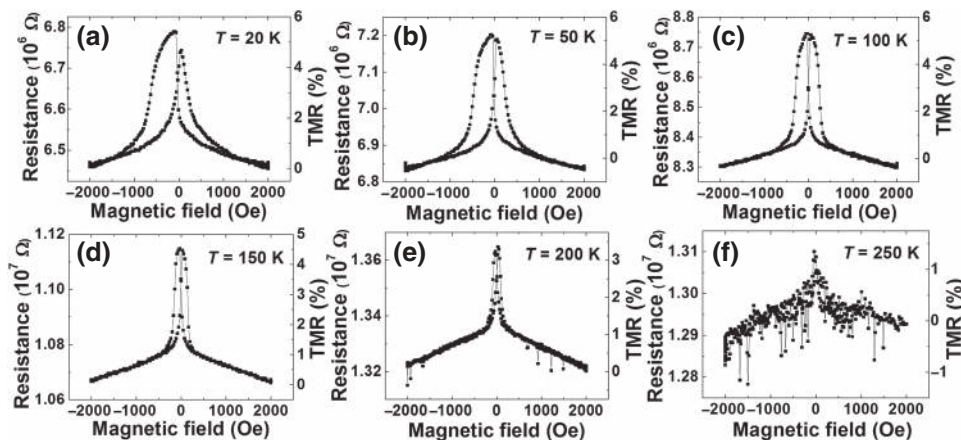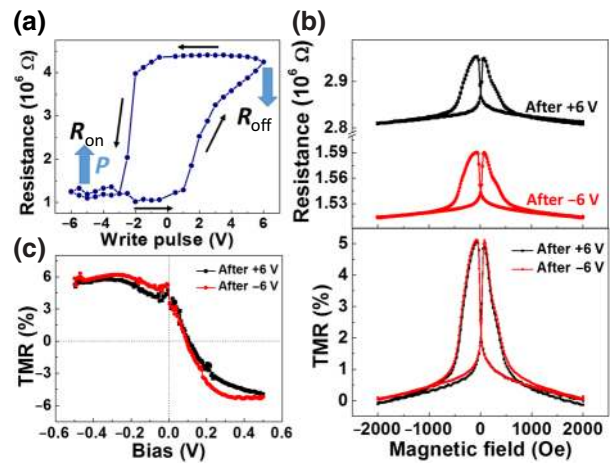

FIG. 5. Combined TMR and TER. (a) A resistance hysteresis loop (read by a voltage of 100 mV) as a function of write pulses with different amplitudes from -6 V to $+6$ V and a width of 500 μs on a junction of size 30×30 μm^2. The blue arrows indicate the orientation of the ferroelectric polarization as up ($P_\uparrow$, toward the Co electrode) and down ($P_\downarrow$, toward the LSMO electrode). (b) The resistance as a function of the magnetic field (upper panel) and the corresponding TMR loops (lower panel) under a bias of -0.2 V at 50 K. (c) The bias-dependent TMR ratio after $+6$ V and -6 V pulses on a junction of size 20×20 μm^2.

such as has been reported for conventional perovskite ferroelectric barriers [6–9,46]. The junction resistance measured under a bias of 0.1 V is plotted as a function of the amplitude of the successive write pulses (500 μs pulse width). A clear hysteresis cycle between a low- (R_{on}) and a high- (R_{off}) resistance state is achieved, with an *on/off* ratio of 440%, defined as R_{off}/R_{on}. The switching voltage between the two states is around 2 V when the write pulse is swept from -6 V to 6 V and around -2 V when going back to -6 V. This is consistent with previous reports, which ascribe the TER effect to the ferroelectric polarization switching [7,20,26,28,30].

We have demonstrated ferroelectric switching in layers of the same materials with thicknesses down to 5 nm

FIG. 4. The TMR ratios of a junction with a size of 10×10 μm^2 under a bias of -0.2 V at different temperatures: (a) 20 K, (b) 50 K, (c) 100 K, (d) 150 K, (e) 200 K, and (f) 250 K, respectively.

in previous work [34]. However, macroscopic polarization switching was not possible in 2-nm-thick layers, like the ones shown here, because of the steep increase of the switching field with decreasing thickness. Therefore, we use piezoelectric force microscopy (PFM) with an applied voltage to the AFM tip similar to that used for the TER measurements to test the local ferroelectric switching. A reversal of the PFM contrast is, indeed, observed in Fig. S3 (see the Supplemental Material [35]) at voltages similar to those required for resistive switching. Nevertheless, in this geometry, electrostatic effects and ionic migration cannot be excluded as the origin of the observed contrast [47,48]. The as-grown state of the HZO films corresponds to the low-resistance state (R_{on}) with the ferroelectric polarization up ($P_\uparrow$), as indicated in Fig. S3 (see the Supplemental Material [35]).

In Fig. 5(b), TMR loops are obtained after $+6$ V (R_{off}) and -6 V (R_{on}) pulses and show both a TMR ratio of around 5.2%, corresponding to TER = 190%. Four resistance states can thus be obtained and switched reversibly using both electrical and magnetic inputs. One can observe that the TMR does not change significantly between the *on* and *off* states. The spin polarization of the tunneling electrons thus appears to be unaffected by the ferroelectric switching, which is different from junctions with perovskite ferroelectric tunnel barriers, such as $PbZr_{0.2}Ti_{0.8}O_3$ (PZT) [25] and $BaTiO_3$ (BTO) [24]. In these systems, it has been reported that, upon switching of the polarization, the induced magnetic moment of the interfacial Ti ion changes significantly due to the hybridization effect at the interface between the tunnel barrier and the FM electrode, thus inducing strong magnetoelectric coupling [25,49,50] In our case, the polarization of the HZO layer is due to the displacement of the oxygen atoms and this hybridization effect cannot be invoked. Furthermore, to study the dependence of the TMR on the bias, I-V curves are measured in both the parallel and antiparallel states. From these measurements, the TMR ratio can be extracted at different bias values, since TMR $= (I_P - I_{AP})/I_{AP}$, where I_{AP} and I_P are the currents in the antiparallel and parallel states, respectively. Figure 5(c) shows that the bias dependence of the TMR ratio is barely affected by the ferroelectric polarization state. This once again proves the stability of the resistance states and also the absence of measurable magnetoelectric coupling [24,25] in this system.

As shown in Fig. 6(a), when a positive bias of 0.2 V is applied on the top electrode Co, an inverse TMR (of around -2.6%) is observed at 50 K, corresponding to a smaller resistance measured in the antiparallel state compared to the parallel one. From the resulting TMR-V curve (red) in Fig. 6(b) at the same temperature, the largest TMR (approximately 6%) is measured at a bias of about -0.3 V. The inverse TMR can be observed above a threshold bias value of around 0.1 V at this temperature. According to Julliere's model [51], the amplitude and sign of the
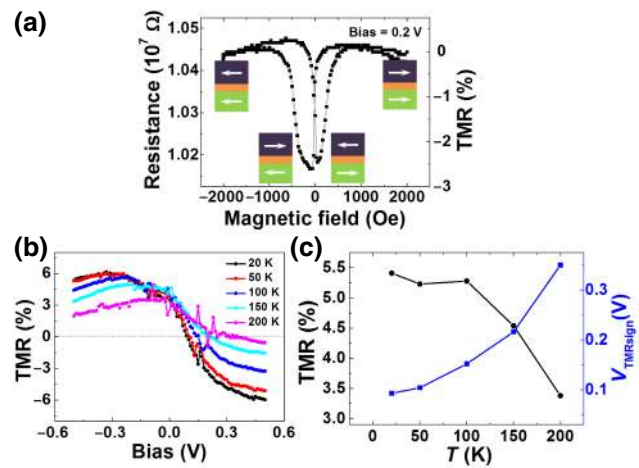

FIG. 6.　Inverse TMR. (a) The TMR loop obtained in a junction of size 10×10 μm^2 under a bias of 0.2 V at 50 K with high (low) resistance in the parallel (antiparallel) state. (b) The bias-dependent TMR from -0.5 V to 0.5 V at different temperatures from 20 K to 200 K. (c) The temperature dependence of both TMR (black, circles) and $V_{TMRsign}$, the voltage needed for TMR sign reversal (blue, squares) in the same junction.

TMR are related to the spin polarization of the density of states (DOS) of the two ferromagnetic layers. In particular, for the case of tunneling between LSMO and Co electrodes, the application of different bias changes the relative position of the DOS of Co and LSMO, as depicted by De Teresa *et al.* [37] for a $SrTiO_3$ barrier. The inverse TMR could also be attributed to the resonant tunneling via localized states in the barrier, which is reported in the Ni/NiO/Co system by Tsymbal *et al.* [52]. By changing the bias on the junction, the position and the width of the resonant states can be tuned. When the energy of localized states in the barrier matches the Fermi energy of the FM electrodes, the TMR is inverted.

Moreover, in the case of the HZO barrier, TMR-V curves are also plotted in Fig. 6(b) at different temperatures. The bias at which the TMR sign changes is defined as $V_{TMRsign}$. Interestingly, we observe that $V_{TMRsign}$ increases with the temperature, from approximately 0.1 V at 20 K to approximately 0.35 V at 200 K, as shown in Fig. 6(c) (in blue line). This could be due to the decreasing spin polarization of LSMO at the interface with HZO with increasing temperature, as the decrease of TMR shows a similar trend [plotted in black in Fig. 6(c) with values extracted from Fig. 4]. It could also be due to the energy of impurity states in the barrier changing with increasing temperature, with the corresponding change of the voltage ($V_{TMRsign}$) needed to align the impurity states with the Fermi energy of the FM electrodes.

We successfully build MFTJs with an ultrathin ferroelectric hafnia-based barrier. The junctions display several appealing characteristics, such as (1) four nonvolatile resistive-memory driven by electric and magnetic fields,

(2) bias-dependent inverse TMR, and (3) memristive behavior. The large band gap and high quality of the HZO tunnel barriers give rise to a remarkable homogeneity in the RA product over all of the measured junctions with different surface areas. This allows us to utilize these ultrathin barriers in standard devices, which is a clear advantage with respect to similarly thin barriers of other materials, which can only be investigated using scanning probes [24,25]. All of the above shows the great potential of this material for multifunctional devices and adaptable electronics.

[1] James F. Scott, *Ferroelectric Memories* (Springer-Verlag Berlin Heidelberg, 2000), Vol. 3.

[2] Thomas Tybell, C. H. Ahn, and J.-M. Triscone, Ferroelectricity in thin perovskite films, Appl. Phys. Lett. **75**, 856 (1999).

[3] Celine Lichtensteiger, Jean-Marc Triscone, Javier Junquera, and Philippe Ghosez, Ferroelectricity and Tetragonality in Ultrathin $PbTiO_3$ Films, Phys. Rev. Lett. **94**, 047603 (2005).

[4] Dillon D. Fong, G. Brian Stephenson, Stephen K. Streiffer, Jeffrey A. Eastman, Orlando Auciello, Paul H. Fuoss, and Carol Thompson, Ferroelectricity in ultrathin perovskite films, Science **304**, 1650 (2004).

[5] Evgeny Y. Tsymbal and Hermann Kohlstedt, Tunneling across a ferroelectric, Science **313**, 181 (2006).

[6] Vincent Garcia, Stephane Fusil, Karim Bouzehouane, Shaima Enouz-Vedrenne, Neil D. Mathur, Agnés Barthélémy, and Manuel Bibes, Giant tunnel electroresistance for non-destructive readout of ferroelectric states, Nature **460**, 81 (2009).

[7] André Chanthbouala, Arnaud Crassous, Vincent Garcia, Karim Bouzehouane, Stéphane Fusil, Xavier Moya, Julie Allibe, Bruno Dlubak, Julie Grollier, Stephane Xavier, Cyrile Deranlot, Amir Moshar, Roger Proksch, Neil D. Mathur, Manuel Bibes, and Agnés Barthélémy, Solid-state memories based on ferroelectric tunnel junctions, Nat. Nanotechnol. **7**, 101 (2012).

[8] Y. W. Yin, J. D. Burton, Young Min Kim, Albina Y. Borisevich, Stephen J. Pennycook, Sang Mo Yang, T. W. Noh, A. Gruverman, X. G. Li, E. Y. Tsymbal, and Q. Li, Enhanced tunnelling electroresistance effect due to a ferroelectrically induced phase transition at a magnetic complex oxide interface, Nat. Mater. **12**, 397 (2013).

[9] Peter Maksymovych, Stephen Jesse, Pu Yu, Ramamoorthy Ramesh, Arthur P. Baddorf, and Sergei V. Kalinin, Polarization control of electron tunneling into ferroelectric surfaces, Science **324**, 1421 (2009).

[10] A. Crassous, V. Garcia, K. Bouzehouane, S. Fusil, A. H. G. Vlooswijk, G. Rispens, B. Noheda, M. Bibes, and A. Barthélémy, Giant tunnel electroresistance with $PbTiO_3$ ferroelectric tunnel barriers, Appl. Phys. Lett. **96**, 042901 (2010).

[11] Zhongqiang Hu, Qian Li, Meiya Li, Qiangwen Wang, Yongdan Zhu, Xiaolian Liu, Xingzhong Zhao, Yun Liu, and Shuxiang Dong, Ferroelectric memristor based on $Pt/BiFeO_3/Nb$-doped $SrTiO_3$ heterostructure, Appl. Phys. Lett. **102**, 102901 (2013).

[12] Hiroyuki Yamada, Vincent Garcia, Stéphane Fusil, Sören Boyn, Maya Marinova, Alexandre Gloter, Stéphane Xavier, Julie Grollier, Eric Jacquet, Cecile Carretero, Cyrile Deranlot, Manuel Bibes, and Agnes Barthélémy, Giant electroresistance of super-tetragonal $BiFeO_3$-based ferroelectric tunnel junctions, ACS Nano **7**, 5385 (2013).

[13] Javier Junquera and Philippe Ghosez, Critical thickness for ferroelectricity in perovskite ultrathin films, Nature **422**, 506 (2003).

[14] T. S. Böscke, J. Müller, D. Bräuhaus, U. Schröder, and U. Böttger, Ferroelectricity in hafnium oxide thin films, Appl. Phys. Lett. **99**, 102903 (2011).

[15] Min Hyuk Park, Young Hwan Lee, Han Joon Kim, Yu Jin Kim, Taehwan Moon, Keum Do Kim, Johannes Mueller, Alfred Kersch, Uwe Schroeder, Thomas Mikolajick, and Cheol Seong Hwang, Ferroelectricity and antiferroelectricity of doped thin HfO_2-based films, Adv. Mater. **27**, 1811 (2015).

[16] J. Müller *et al.*, in *2013 IEEE International Electron Devices Meeting* (IEEE, Washington, DC, 2013), p. 10.

[17] Min Hyuk Park, Han Joon Kim, Yu Jin Kim, Woongkyu Lee, Taehwan Moon, and Cheol Seong Hwang, Evolution of phases and ferroelectric properties of thin $Hf_{0.5}Zr_{0.5}O_2$ films according to the thickness and annealing temperature, Appl. Phys. Lett. **102**, 242905 (2013).

[18] J. Robertson, High dielectric constant oxides, Eur. Phys. J. Appl. Phys. **28**, 265 (2004).

[19] Julian P. Velev, Chun-Gang Duan, J. D. Burton, Alexander Z. Smogunov, Manish K. Niranjan, Erio Tosatti, S. S. Jaswal, and Evgeny Y. Tsymbal, Magnetic tunnel junctions with ferroelectric barriers: Prediction of four resistance states from first principles, Nano Lett. **9**, 427 (2008).

[20] Vincent Garcia and Manuel Bibes, Ferroelectric tunnel junctions for information storage and processing, Nat. Commun. **5**, 4289 (2014).

[21] Evgeny Y. Tsymbal, Alexei Gruverman, Vincent Garcia, Manuel Bibes, and A. Barthélémy, Ferroelectric and multiferroic tunnel junctions, MRS Bull. **37**, 138 (2012).

[22] Mario Norberto Baibich, Jean Marc Broto, Albert Fert, F. Nguyen Van Dau, Frédéric Petroff, P. Etienne, G. Creuzet, A. Friederich, and J. Chazelas, Giant Magnetoresistance of (001)Fe/(001)Cr Magnetic Superlattices, Phys. Rev. Lett. **61**, 2472 (1988).

[23] Andy Quindeau, Ignasi Fina, Xavi Marti, Geanina Apachitei, Pilar Ferrer, Chris Nicklin, Eckhard Pippel, Dietrich Hesse, and Marin Alexe, Four-state ferroelectric spin-valve, Sci. Rep. **5**, 9749 (2015).

[24] V. Garcia, M. Bibes, L. Bocher, S. Valencia, F. Kronast, A. Crassous, X. Moya, S. Enouz-Vedrenne, A. Gloter, D. Imhoff, C. Deranlot, N. D. Mathur, S. Fusil, K. Bouzehouane, and A. Barthélémy, Ferroelectric control of spin polarization, Science **327**, 1106 (2010).

[25] D. Pantel, S. Goetze, D. Hesse, and M. Alexe, Reversible electrical switching of spin polarization in multiferroic tunnel junctions, Nat. Mater. **11,** 289 (2012).

[26] F. Ambriz-Vargas, G. Kolhatkar, R. Thomas, R. Nouar, A. Sarkissian, C. Gomez-Yáñez, M. A. Gauthier, and A. Ruediger, Tunneling electroresistance effect in a Pt/Hf$_{0.5}$Zr$_{0.5}$O$_2$/Pt structure, Appl. Phys. Lett. **110,** 093106 (2017).

[27] Shosuke Fujii, Yuuichi Kamimuta, Tsunehiro Ino, Yasushi Nakasaki, Riichiro Takaishi, and Masumi Saitoh, in *2016 IEEE Symposium on VLSI Technology* (IEEE, Honolulu, Hawaii, 2016), p. 1.

[28] Lin Chen, Tian-Yu Wang, Ya-Wei Dai, Ming-Yang Cha, Hao Zhu, Qing-Qing Sun, Shi-Jin Ding, Peng Zhou, Leon Chua, and David Wei Zhang, Ultra-low power *Hf*$_{0.5}$Zr$_{0.5}$O$_2$ based ferroelectric tunnel junction synapses for hardware neural network applications, Nanoscale **10,** 15826 (2018).

[29] Fabian Ambriz-Vargas, Gitanjali Kolhatkar, Maxime Broyer, Azza Hadj-Youssef, Rafik Nouar, Andranik Sarkissian, Reji Thomas, Carlos Gomez-Yáñez, Marc A. Gauthier, and Andreas Ruediger, A complementary metal oxide semiconductor process-compatible ferroelectric tunnel junction, ACS Appl. Mater. Interfaces **9,** 13262 (2017).

[30] A. Chouprik, A. Chernikova, A. Markeev, V. Mikheev, D. Negrov, M. Spiridonov, S. Zarubin, and A. Zenkevich, Electron transport across ultrathin ferroelectric Hf$_{0.5}$Zr$_{0.5}$O$_2$ films on Si, Microelectron. Eng. **178,** 250 (2017).

[31] Youngin Goh and Sanghun Jeon, Enhanced tunneling electroresistance effects in HfZrO-based ferroelectric tunnel junctions by high-pressure nitrogen annealing, Appl. Phys. Lett. **113,** 052905 (2018).

[32] C. L. Platt, B. Dieny, and A. E. Berkowitz, Spin-dependent tunneling in HfO$_2$ tunnel junctions, Appl. Phys. Lett. **69,** 2291 (1996).

[33] Savio Fabretti, Robert Zierold, Kornelius Nielsch, Carmen Voigt, Carsten Ronning, Patrick Peretzki, Michael Seibt, and Andy Thomas, Temperature and bias-voltage dependence of atomic-layer-deposited HfO$_2$-based magnetic tunnel junctions, Appl. Phys. Lett. **105,** 132405 (2014).

[34] Yingfen Wei, Pavan Nukala, Mart Salverda, Sylvia Matzen, Hong Jian Zhao, Jamo Momand, Arnoud S. Everhardt, Guillaume Agnus, Graeme R. Blake, Philippe Lecoeur, Bart J. Kooi, Jorge Iniguez, Brahim Dkhil, and Beatriz Noheda, A rhombohedral ferroelectric phase in epitaxially strained Hf$_{0.5}$Zr$_{0.5}$O$_2$ thin films, Nat. Mater. **17,** 1095 (2018).

[35] See the Supplemental Material at http://link.aps.org/supplemental/10.1103/PhysRevApplied.12.031001 for an EDS image of the junction, TEM images across different regions, and AFM topography, as well as PFM images.

[36] W. F. Brinkman, R. C. Dynes, and J. M. Rowell, Tunneling conductance of asymmetrical barriers, J. Appl. Phys. **41,** 1915 (1970).

[37] J. M. De Teresa, A. Barthélémy, A. Fert, J. P. Contour, R. Lyonnet, F. Montaigne, P. Seneor, and A. Vaures, Inverse Tunnel Magnetoresistance in Co/SrTio$_3$/La$_{0.7}$Sr$_{0.3}$MnO$_3$: New Ideas on Spin-Polarized Tunneling, Phys. Rev. Lett. **82,** 4288 (1999).

[38] Jose Maria De Teresa, Agnes Barthélémy, Albert Fert, Jean Pierre Contour, François Montaigne, and Pierre Seneor, Role of metal-oxide interface in determining the spin polarization of magnetic tunnel junctions, Science **286,** 507 (1999).

[39] V. Garcia, M. Bibes, J.-L. Maurice, E. Jacquet, K. Bouzehouane, J.-P. Contour, and A. Barthélémy, Spin-dependent tunneling through high-*k* LaAlO$_3$, Appl. Phys. Lett. **87,** 212501 (2005).

[40] Andy Quindeau, Ignasi Fina, Xavi Marti, Geanina Apachitei, Pilar Ferrer, Chris Nicklin, Eckhard Pippel, Dietrich Hesse, and Marin Alexe, Four-state ferroelectric spin-valve, Sci. Rep. **5,** 9749 (2015).

[41] V. Garcia, M. Bibes, A. Barthélémy, M. Bowen, E. Jacquet, J.-P. Contour, and A. Fert, Temperature dependence of the interfacial spin polarization of La$_{2/3}$Sr$_{1/3}$MnO$_3$, Phys. Rev. B **69,** 052403 (2004).

[42] Yu Lu, X. W. Li, G. Q. Gong, Gang Xiao, A. Gupta, Ph Lecoeur, J. Z. Sun, Y. Y. Wang, and V. P. Dravid, Large magnetotunneling effect at low magnetic fields in micrometer-scale epitaxial La$_{0.67}$Sr$_{0.33}$MnO$_3$ tunnel junctions, Phys. Rev. B **54,** R8357 (1996).

[43] J.-H. Park, E. Vescovo, H.-J. Kim, C. Kwon, R. Ramesh, and T. Venkatesan, Magnetic Properties at Surface Boundary of a Half-Metallic Ferromagnet La$_{0.7}$Sr$_{0.3}$MnO$_3$, Phys. Rev. Lett. **81,** 1953 (1998).

[44] A. M. Haghiri-Gosnet, M. Koubaa, A. F. Santander-Syro, R. P. S. M. Lobo, Ph Lecoeur, and B. Mercey, Metallic nature of strained thin single-crystal La$_{2/3}$Sr$_{1/3}$MnO$_3$ films, Phys. Rev. B **78,** 115118 (2008).

[45] J. Z. Sun, L. Krusin-Elbaum, P. R. Duncombe, A. Gupta, and R. B. Laibowitz, Temperature dependent, non-ohmic magnetoresistance in doped perovskite manganate trilayer junctions, Appl. Phys. Lett. **70,** 1769 (1997).

[46] André Chanthbouala, Vincent Garcia, Ryan O. Cherifi, Karim Bouzehouane, Stéphane Fusil, Xavier Moya, Stéphane Xavier, Hiroyuki Yamada, Cyrile Deranlot, Neil D. Mathur, Manuel Bibes, Agnes Barthélémy, and Julie Grollier, A ferroelectric memristor, Nat. Mater. **11,** 860 (2012).

[47] Nina Balke, Stephen Jesse, Qian Li, Petro Maksymovych, M. Baris Okatan, Evgheni Strelcov, Alexander Tselev, and Sergei V. Kalinin, Current and surface charge modified hysteresis loops in ferroelectric thin films, J. Appl. Phys. **118,** 072013 (2015).

[48] Nina Balke, Petro Maksymovych, Stephen Jesse, Andreas Herklotz, Alexander Tselev, Chang-Beom Eom, Ivan I. Kravchenko, Pu Yu, and Sergei V. Kalinin, Differentiating ferroelectric and nonferroelectric electromechanical effects with scanning probe microscopy, ACS Nano **9,** 6484 (2015).

[49] M. Fechner, S. Ostanin, and I. Mertig, Effect of oxidation of the ultrathin fe electrode material on the strength of magnetoelectric coupling in composite multiferroics, Phys. Rev. B **80,** 094405 (2009).

[50] Maznichenko Fechner, I. V. Maznichenko, S. Ostanin, A. Ernst, J. Henk, P. Bruno, and Ingrid Mertig, Magnetic phase transition in two-phase multiferroics predicted from first principles, Phys. Rev. B **78,** 212406 (2008).

[51] Michel Julliere, Tunneling between ferromagnetic films, Phys. Lett. A **54,** 225 (1975).

[52] E. Y. Tsymbal, A. Sokolov, I. F. Sabirianov, and B. Doudin, Resonant Inversion of Tunneling Magnetoresistance, Phys. Rev. Lett. **90,** 186602 (2003).